Spring 5-15-2020

Density Functional Theory Calculations of Al doped Hafnia for Different Crystal Symmetry Configurations

Joshua Steier
joshua.steier@student.shu.edu

Density Functional Theory Calculations of Al doped Hafnia for Different Crystal Symmetry Configurations

Master's Thesis

Submitted to the faculty of the Department of Physics

in the School of Arts and Sciences as partial fulfillment of the requirements for the degree of

Master's of Science.

Seton Hall University

400 South Orange Avenue

South Orange, New Jersey 07079

Joshua J. Steier

May 2020

We certify that we have read this dissertation and that in our opinion it is adequate in scientific scope and quality as a dissertation for the degree of Masters of Science.

APPROVED

May 4th 2020

Mehmet Alper Sahiner, Ph.D. Date

Research Mentor and, Member of Dissertation Committee

Chair, Department of Physics

Seton Hall University

May 4, 2020

Stephen P. Kelty, Ph.D. Date

Research Mentor, Member of Dissertation Committee

Chair, Department of Chemistry and Biochemistry

Seton Hall University

05/04/20

Weining Wang, Ph.D. Date

Member of Dissertation Committee

Seton Hall University

Acknowledgements

I would firstly like to acknowledge the guidance and mentorship from Dr. Stephen Kelty during this project. Dr. Kelty has always been a great mentor and taught me so much during our time working together. I am indebted to him for his kindness and valuable insight, and this work would not be possible without him. I look forward to keeping in touch, and hopefully will have collaborations in the future.

Next, I would like to acknowledge the guidance of Dr. Mehmet Alper Sahiner. Dr. Sahiner always provides valuable insight and gives great advice when it is most needed. He is a great research mentor due to his high knowledgeability and extreme kindness. I am greatly appreciative of all the guidance and constant feedback I have received during this project.

Further, I would like to acknowledge the assistance and mentorship of Dr. Anthony Troha. Dr. Troha is a fantastic mentor who spent countless days and nights granting me knowledge on this research topic. He serves as a constant source of inspiration as my motivation to finish this work would not exist without him. He is an extremely kind soul and there is no one who has contributed more to my growth as a researcher than he has. I learned valuable lessons in research and in life from his tutelage, and I only hope to keep in touch and collaborate in the future.

I would also like to acknowledge the boundless support from my students and friends. My students have always been my most loyal companions and have been presented to support all my endeavors. They allow me to share my passion for physics and listen closely when I talk about my research. They are a constant source of inspiration and the teacher is nothing without the students. As I am constantly teaching them, so too are they constantly teaching me. Each and every one of my students has provided me with more knowledge and growth during this project.

My friends have always been at my side when difficulties arise in research. One of my best friends, Alexander Law contributed as emotional support alongside another best friends, Jared Savastano and Jeffery Raab during this time and I'm eternally grateful. Thank you, to all my students and friends for your endless support.

Further, I would like to acknowledge the mentorship of Dr. Kobi Abayomi. Dr. Abayomi has always been a staunch supporter at almost every significant event in my collegiate career. Kobi pushed for my applications to graduate school and assisted in expanding my network which has been crucial for employment. Kobi is a humble man with a beautiful mind and is one of my inspirations and raisons d'etre. I am extremely grateful for all the life lessons, research methods, and motivation to succeed in all of my endeavors.

Lastly, I would like to acknowledge the assistance and guidance of Rory Vander Valk. Rory has been outstandingly helpful in terms of understanding basic Density Functional Theory and determining which pseudopotentials to use. His advice on how to conduct this research in the first place was excellent and I am grateful for it.

The research conducted for this thesis would not have been possible without the physics master's program and I am grateful for being one of the first students to participate in the physics master's program at Seton Hall University. I am grateful for the teaching assistant position and tuition wavier which helped ease any financial burden and allow me to obtain this degree.

Table of Contents

List of Tables

List of Figures

Abstract

Dogan et al.[1], investigated the causes of ferroelectricity in doped hafnia using ab initio methods. Similarly, we investigated the stability of Al doped hafnia using quantum mechanical methods.

There are many different phases of Hafnia: monoclinic, tetragonal, cubic and orthorhombic. Starting with the monoclinic phase of Hafnia, Hafnia undergoes phase transitions which result in different space groups. The temperature at which the tetragonal phase is induced is 2000 K and cubic phase is induced at 2900 K[1]. Different dielectric constants vary from phase to phase. The average dielectric constants are highest for the cubic and tetragonal phases. In order to force a high temperature phase to be stable in Hafnia, one would need to introduce cation dopants.

The polar orthorhombic phase is well known to exhibit ferroelectricity. Since inducing this phase with about 40 GPa it is more effective to induce a ferroelectric phase in Hafnia via doping methods. Doping methods for Hafnia are well established in [1] and demonstrated for Si, Ge, La and other elements. The rhombohedral phase is of interest and investigated first in [35]. Since ferroelectricity in the rhombohedral phase is difficult to stabilize, dopants are introduced analogously to the orthorhombic case. In this work, we doped the monoclinic, tetragonal, orthorhombic and rhombohedral phase of Hafnia with Al to investigate the effect of dopants on ferroelectricity and relevant EXAFS data was also produced.

Using plane wave density functional theory, the tetragonal, orthorhombic, and trigonal phases of aluminum doped hafnia were geometrically optimized. The resulting 3 percent, 6 percent, and 7

percent Al doped hafnia structures were used for generating expected EXAFS spectra for experimental data analysis and validation. Specifically, these DFT calculated structures are going to be used in the non-linear least square EXAFS fits of the thin films HfAlO2.

Keywords: Density functional theory, ferroelectricity, doped hafnia

Introduction

Section I: Introduction to Quantum Mechanics

Quantum mechanics necessarily developed from the failures of classical physics. Since density functional theory is a quantum mechanical method, we will first make some remarks about quantum mechanics.

Niels Bohr investigated the quantum nature of the electron. He found that electrons follow specified paths called orbitals and on these orbitals electrons do not radiate energy. Further, he found

$$E = \frac{-13.6eV}{n^2} (1)$$

and these energies are negative since these are bound states of an electron with nucleus with reference to the ground energy state when they are infinitely apart.

Further, he proposed that electrons and move between orbitals by absorbing or emitting a quanta of energy. [2]

$$\Delta E = -13.6\left(\frac{1}{n_1^2} - \frac{1}{n_2^2}\right) (2)$$

Planck reported that blackbody radiation could be explained nicely only if the radiation energies were discrete. Both Planck and Bohr were looking at the quantum nature of electrons from different perspectives.

The wave-particle duality of electrons is also an important development in quantum mechanics. De Brogile pioneered the development that an electron is both a wave and a particle. The frequency is directly proportional to the particle's kinetic energy:

$p = \frac{h}{\lambda}$ (3) and $E = hv$.(4)

p is momentum, h is Planck's constant, λ is the wavelength, v is the frequency.

Heisenberg is well known for the uncertainty principle he developed. If one measures the position of an electron one cannot know the momentum and vice versa. This means that when dealing with quantum mechanical methods, such as DFT, all calculations are really probabilities. For example, electron positions are represented as electron densities that are probabilities of finding electrons in a finite volume element. Fortunately, during the quantum mechanical calculations, the uncertainty principle is not involved since the system is time independent, and errors of the methods are far greater than the uncertainly involved. [2]

Schrödinger(name needs to be adjusted), also engendered the rise of quantum mechanics. He developed a wave equation:

$\hat{H}\psi = E\psi$.(5)

Where $\hat{H}$ is the Hamiltonian operator, ψ is the wave function and E is the system's energy.

It is helpful to look at the Schrodinger equation from the wave-particle duality proposed by De Brogile.[3]

Looking at the particle description:

Since $E = \frac{1}{2}mv^2 + V$(6)

then $v = \left(\frac{2(E-V)}{m}\right)^{\frac{1}{2}}$(7)

and $p = mv = \left(2m(E-V)\right)^{\frac{1}{2}}$.(8)

Now looking at the wave description:

From $\frac{d^2\psi}{dx^2} = -\left(\frac{2\pi}{\lambda}\right)^2$(9)

rearranging gives $\left(\frac{2\pi}{\lambda}\right)^2 = \frac{-1}{\psi}d^2\psi dx^2$(10)

or $\frac{1}{\lambda} = \left(\frac{-1}{4\pi^2\psi}\frac{d^2\psi}{dx^2}\right)^{\frac{1}{2}}$(11)

Then, using de Broglie's relation(3):

$$p = h\left(\frac{1}{\lambda}\right)$$

$$2m(E-V)^{\frac{1}{2}} = h\left(\frac{-1}{4\pi^2\psi}\frac{d^2\psi}{dx^2}\right)^{\frac{1}{2}} (12)$$

$$2m(E-V) = \left(\frac{-h^2}{4\pi^2\psi}\frac{d^2\psi}{dx^2}\right) (13)$$

$$(E - V)\psi = \frac{-h^2}{8\pi^2 m}\frac{d^2\psi}{dx^2}(14)$$

$$\frac{-h^2}{8\pi^2 m}\frac{d^2}{dx^2}\psi + V\psi = E(15)$$

Therefore,

$$\left(\frac{-h^2}{8\pi^2 m}\frac{d^2}{dx^2} + V\right)\psi = E(16)$$

Thus, using de Broglie's relation(3) wave-particle duality can be used to derive the Schrodinger equation.

The wave function describes the quantum state o a set of particles in an isolated system.

An operator does a mathematical operation on a variable, e.g. a derivative $\frac{d}{dx}$.

It is important to note that any observable in quantum mechanics is represented by an operator.

Operators can also be non-commutative meaning they cannot be measured simultaneously or known precisely. Consider the example of position and linear momentum in the x direction.

If two operators $\widehat{A}$ and $\widehat{B}$ commute then:

$$\left[\hat{A}, \hat{B}\right] = 0$$

Where $\left[\hat{A}, \hat{B}\right] = \widehat{A\hat{B}} - \widehat{B\hat{A}}$. [4]

A Hermitian operator is linear operator $\hat{A}$ that obeys:

$$\int f_m^* \hat{A} f_n d\tau = \int f_n \left(\hat{A} f_m\right)^* d$$

A linear operator is an operator $\hat{A}$ that obeys the following properties:

1). $\hat{A}(f(x) + g(x)) = \hat{A}f(x) + \hat{A}g(x)$

2). $\hat{A}(cf(x)) = c\hat{A}f(x)$

A unitary operator is an operator $\widehat{U}$ for which $\widehat{\mathrm{U}} = \mathrm{U}^t$

There are several important postulates of quantum mechanics:

1). The state of the system is given by the wave function:

$$\psi(x, y, z)$$

2). All observables are represented by operators commuting:

$$[\hat{x},\ p] = i\hbar$$

3). The mean value of an observable is the expectation value:

$$\langle \Omega \rangle = \frac{\int \psi^* \, \Omega \psi dr}{\int \psi^* \, \psi dr}$$

A plane wave is a wave function that propagates perpendicularly to wave fronts with a constant frequency.

A standing wave is a wave function which does not propagate but vibrates up and down in place.

In an effort to calculate various electronic properties, one must consider the interactions involving electrons in the system.

This is intrinsically difficult since the interactions between electrons are too complex to consider numerically, and this is termed the many-body problem.

Early efforts to mitigate this problem were investigated by Hartree. The Hartree method utilized a mean electron field to calculate electronic properties of complex systems.

The Hartree method had two main failures:

1). It does not follow the antisymmetry principle and Pauli's exclusion principle.

2). It does not count the exchange and correlation energies coming from the n- electron nature of actual systems.

The Hartree method was then refined to become the Hartree-Fock method.

The Hartree-Fock method improved upon the Hartree method in several important ways. First, the wave function is expressed in the form of a Slater determinant, which makes the wave function anti-symmetric, thus satisfying a previous approximation.

A Slater determinant is a mathematical expression of the wave function using determinants that satisfies the antisymmetry principle. Therefore the use of a Slater determinant also satisfies the Pauli exclusion principle.

Since electrons are interacting, expressing the wave function as a single Slater determinant is also an approximation, which is subject to a systematic improvement to the exact function. The variational principle is used in this regard.

In quantum mechanics, there is one ground-state energy and any energy lower than this cannot exist as determined through the variational principle.

Therefore, if one minimizes the system energy with respect to the wave function, the energy must end at the ground-state energy.

The variational principle can be written as:

$$0 = \delta\left(\int \Psi \hat{H} \Psi dr\right).$$

Section II: Density Functional Theory

The Hartree-Fock method adopts a self-consistent procedure:

1). Choose a proper set of n wave functions, such as of hydrogen for an atomic calculation and a linear combination of atomic orbitals for solids.

2). Calculate the electron density: $\rho(r')$

3). Calculate the three energy terms of $\hat{H}$ for n electrons.

4). Insert these values into the wave equations and solve to have a set of E_i and a new set of wave functions.

5). Repeat the above process until self-consistency is reached and input wavefunctions and output wavefunctions become the same in a certain range of error.

Density Functional Theory calculations have been used to provide insight on the ferroelectric effects of doped Hafnia. Density Functional Theory is widely used because it greatly simplifies the n-electron problem. Instead of treating the electrons as an electron density. An electron density is the number of electrons per unit volume at a given point. In DFT, the electron density gives all of the information in an n-electron system, in this sense it plays a similar role to the wave function. Assuming the electrons do not interact with one another, one can write the electron density as:

$$\rho(r) = \sum_i |\phi_i(r)|^2 = 2\sum_i^{occ} |\phi_i(r)|^2 . (1)$$

Where ϕ_i are the KS orbitals. KS orbitals are solutions to the KS equations:

$$\left(\frac{-\hbar^2}{2m}\nabla^2 + v_{eff}(r)\right)\phi_i(r) = \epsilon_i\phi_i(r). (2)$$

Here, ϵ_1 is the orbital energy of the corresponding Kohn-Sham orbital, ϕ_i, and the electron density is given above as (1).

Another important feature of DFT is the Hohenberg-Kohn theorems, in which the energies and potentials of the system are postulated to be electron density functionals, where a functional is a function of a function.

The first Hohenberg-Kohn theorem states that there exists a unique external potential, U_{ext} determined solely by the ground state electron density.

One should note that the internal potential energy is independent of the system.

The reasoning behind the first theorem goes as follows:

1). In a system at the ground state, electron density alone can define an external potential and vice versa.

2). Internal energy, which is density dependent is a universal functional $F[\rho(r)]$ and is the same for all systems whereas the external potential depends on the kind of nuclei involved.

3). Hamiltonians must differ by the external potential

4). Electron density defines external potential for the Hamiltonian, wave function and all ground state properties.

We also note that$F[\rho(r)] = \langle\psi|\hat{T} + V_{e-e}|\psi\rangle$ and the expectation value of any operator $\hat{O}$ is a unique functional of the density: $\langle\hat{O}\rangle = O_n[\rho] = \langle\psi_n[\rho]|\hat{O}|\psi_n[\rho]\rangle$.

The second Hohenberg-Kohn theorem demonstrates that there is a way to search to the ground state via the variational principle:

$$E_r[\rho'(r)] = F[\rho(r)] + E_{ext}[\rho(r)] \geq E_{gs}.$$

Alternatively:

$$E_r[\rho'(r)] = F[\rho(r)] + \int_{vext} (r)\rho'(r)dr \geq E_0.$$

It is important to note that the functional delivers the ground state energy of the system if and only if the input density is a true ground state density.

A typical DFT scheme specifically for VASP is detailed in figure

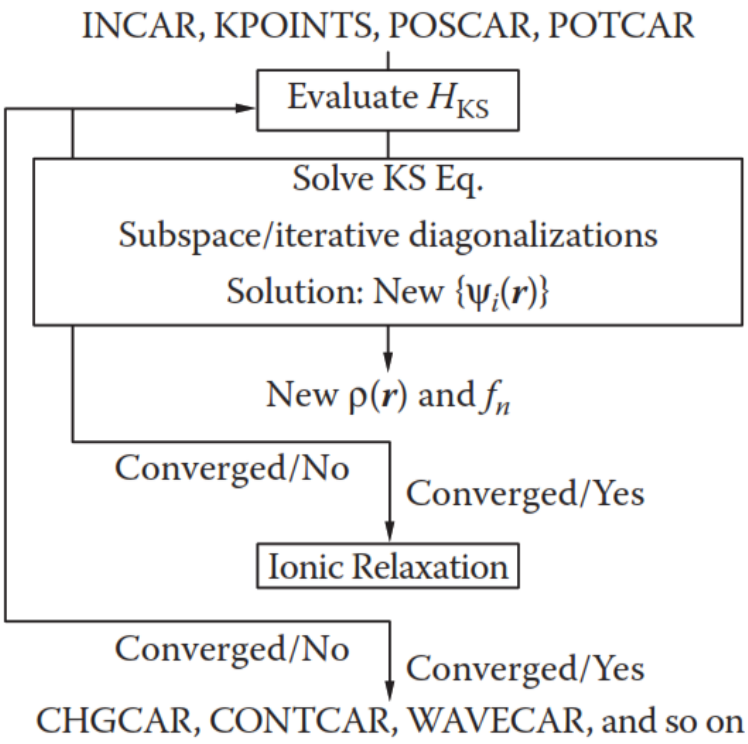

Figure 1. General flow of VASP

In order to discuss PAW potentials and other methods used in this work, we must briefly discuss pseudopotentials. A pseudopotential mimics the behavior of an actual potential. In this frame, the electrons are divided into two groups in terms of contributions, which freezes the nucleus and core electrons together, pseudizing the valence wave functions. Since we are primarily concerned with the valence electrons, these approximations do not hinder our calculations. The core electrons in an atomic system have minimal contribution to bonding when isolated atoms are brought together to form a molecule or crystal. In contrast, the valence electrons have stronger contributions to bonding, ionization, conduction, and band formation. In the frozen-core approximation, which is a computational approach, the core electrons are

removed from the picture and we focus on valence electrons. The wave function must be orthogonal and unique, thus obeying Pauli's exclusion principle. Thus, when the wave function for a valence electron passes by a highly localized core region, it oscillates rapidly and is orthogonal to the core states. It is inherently difficult to classify these curves and so we use the frozen-core approximation. In this way the system is said to be pseudized. The steps involving pseudization is the following: 1). Select an atom as the reference state and the formulated pseudopotential can have both transferable and additive properties in application to different systems. 2). Calculate the exact all electron potential, wave function, and energy by the DFT calculation with the use of spherical symmetry, the core electrons are frozen. 3). Choose r_c to make the core ($r < r_c$) 4). When $r = r_c$, the first and second derivatives of the wave functions are equal. 5). When $r > r_c$ the pseudo and all electron wave functions are exactly the same. 6). The eigenvalues of the smooth pseudo and original wave functions are the same. 7). A pseudopotential is generated from the pseudo wave function and is typically parametrized in spherical Bessel or Gaussian functions. It is important to note that the energies from these pseudopotentials are not the same as ground state energies.

There are many different types of pseudopotentials. We will discuss three basic types: norm-conserving pseudopotentials, ultrasoft pseudopotentials, and projected-augmented wave potentials. In the norm-conserving pseudopotentials, the pseudo and all electron charge densities within the core are equal. (include relevant equations) For ultrasoft pseudopotentials we disregard the norm-conserving condition and make the wave function look like an upside-down bowl. Ultrasoft pseudopotentials only give valence charge densities and not total charge densities. Projected augmented wave potentials

Section III: Introduction to EXAFS

When a system is disturbed, it can exist as a superposition of different possibilities. When the system is measured in some way, the wave function collapses and falls on the possibilities. Since the system exists as a superposition of possibilities with each having its own probability, how do we know which state might be the final state? According to Fermis Golden Rule[16], the probability of each possibility coming to pass depends on the similarity of the proposed final state to the indeterminate state prior to the measurement, the more similar it is the more likely it is.[15]

EXAFS is a commonly used technique to understand and characterize the structure of a material via its electronic properties.[13] EXAFS stands for Extended X-Ray Absorption Fine Structure. EXAFS is a specific region which comes from the XAS, where XAS stands for X-Ray Absorption Spectrum. The other portion of the spectrum from XAS is known as XANES, which stands for X-Ray Absorption Near Edge Structure. In this thesis, we will focus on understanding EXAFS since it was generated as a part of our results. The absorption coefficient will be the central player in understanding how EXAFS works. EXAFS spectroscopy refers to the measurement of the X-ray absorption coefficient μ as a function of photon energy E above the threshold of an absorption edge.[13] The absorption coefficient, given as μ is calculated through $\mu = ln\left(\frac{I_0}{I}\right)$, where$I_0$ and I are the intensities of the incident and transmitted beams, respectively.

Like other forms of light, the intensity of an x-ray is proportional to the number of photons. X-rays are traditionally generated by deceleration of fast moving electrons at a target material. Also if an X-ray tube contains accelerating electrons with an excitation voltage V and goes through a metal target, the maximum frequency of X-rays emitted by Bremsstrahlung is given by the Duane-Hunt law[13]:

$V_{max} = \frac{eV}{h}$, which corresponds to a minimum wavelength: $\lambda_{min} = \frac{hc}{eV}$. λ_{min} represents the shortest wavelength possible for an applied accelerating voltage V since not all the electrons lose energy through this method. Bremsstrahlung is the electromagnetic radiation produced from deacceleration of a charged particle. Magnetobremsstrahlung describes this interaction when magnetic fields are also involved. In 1905, Einstein's paper on the photoelectric effect as published, thus enabling the description of an ejection of an electron from an atom by the absorption of a photon. One should note that when electrons are knocked out of the inner atomic orbital a vacancy is created in the core shell. Electrons in the high energy levels will cascade down and characteristic lines are formed. The wavelength of characteristic lines decreases with increasing atomic number of the material. The maximum kinetic energy of an emitted photoelectron from a material is given by:[13]

$KE_{max} = \frac{1}{2}mv^2 = E - E_0$, where $E = hv$ is the quantized energy of the incident photons and $E_0 = e\phi$ is the threshold energy where ϕ is the work function. In other words, E_0 is the minimum energy required to eject an electron from a particular atomic or molecular orbital.

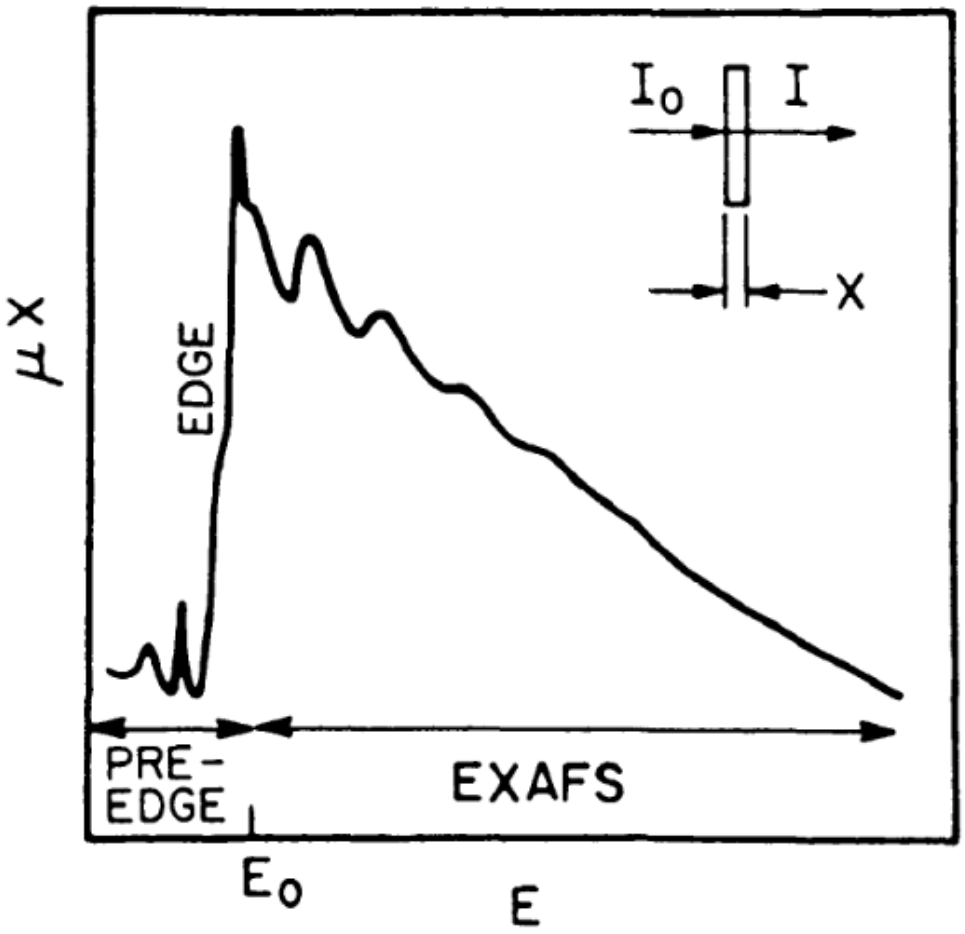

Figure 2. Pre-edge, Edge and EXAFS[13]

]

Continuous spectrum X-ray radiation are produced when the kinetic energy of charged particles is converted to radiation. One important source of continuous spectrum lines is from synchrotron radiation. Synchrotron radiation is emitted when charged particles such as electrons or positrons travel with a speed approaching that of light in curved paths in a magnetic field.[13] There are several advantages to synchrotron radiation which consist of: 1). High intensity; 2). Tunability over a wide energy range; 3). High collimation; 4). Plane-polarization; 5). Precisely pulsed time

structure. X- rays can be characterized as hard or soft. For hard X-rays, the spectrum spans from a few KeV to about 100 KeV. Soft X-rays cover the range from hundreds of eV to a few KeV.

There are different types of transitions that can occur when photons interact with electrons. An electronic transition is when electrons move from one energy level to another. [13] A dipole transition occurs when electrons are moved from one energy level to another. The probability that this transition occurs is called the dipole transition probability.

$hv = E_f - E_i$,where hv is one quantum of electromagnetic raditation, E_f is the energy of the final orbital states and E_i is the energy of the initial states. The dipole transition probability is given as:

X= $e < n'l'm's'|x|nlms >$

$Y = e < n'l'm's'|y|nlms >$

Z= $e < n'l'm's'|z|nlms >$

It is important to note that in a dipole transition, the charge distributions in the initial and final states are different. A dipole transition can be coupled with electromagnetic radiation and put or take energy from an electromagnetic field. Resonance transitions are another important class of transitions. A resonance transition is a transition in which resonant absorption occurs. Resonant absorption is the absorption of electromagnetic energy at a frequency such that the photon energy is equal to the quantum excitation energy of the absorbing system [13]. Characteristic x-rays are emitted when outer-shell electrons fill a vacancy in the inner shell, releasing x-rays that are characteristic to each element[13]. Characteristic x-rays are important because they are used to identify specific elements from which they are emitted. The frequencies of characteristic x-ray lines follow Moseley's law:

$K_\alpha v = k^2(Z - \sigma)^2$, [13]

lines are related to the atomic number Z. Moseley performed an empirical fit on the x-ray frequencies and found the relation above(number). Further, the results can be explained by the Bohr model. The Bohr model is an atomic model that proposes a small nucleus in the center of an atom surrounded by concentric electron shells where electrons obey the Aufbau principle. The Aufbau principle describes the method in which electrons fill shells and subshells.

If an electron from an occupied level goes to an unoccupied level by the absorption of a photon, an absorption spectrum is created. An absorption edge which is a spike in the absorption spectrum, comes from electrons that are excited from core to continuum. Further, a threshold energy is the minimum photon energy that is required to eject an electron out of a state:

$E_0 = hv_0$, which is also the absolute binding energy of the electron.

X -rays interacting with matter lose intensity as photons travel through the matter.

$dI = -\mu I dx$ is the governing equation of the intensity, I, where dI is the change in intensity, μ is the linear absorption coefficient and dx is the change in thickness. If we integrate equation(number) we obtain:

$\frac{I}{I_0} = e^{-\mu}$ where I and I_0 are the incident and transmitted x-ray intensities.

μ in most cases can be approximated as: $\frac{\rho Z^4}{AE^3}$ where ρ is the sample density, Z is the atomic number, A is the atomic mass and x-ray energy is E.[13]

As photon energy increases, the absorption coefficient decreases, and intensity decreases until a critical wavelength is reached where the absorption coefficient increases substantially. The increase corresponds to the ejection of a core electron and results in the absorption edge.

When X-rays interact with matter there are several types of interactions that might occur. X-ray absorption events are of interest to us. These events occur when a photon incident on a sample interacts with electrons and gives up all its energy, which causes the photon to disappear in the process. Electrons transition from lower atomic energy levels go to higher levels which in turn leave vacancies in the lower levels which are filled by electrons moving down to the lower energy level. The transition from a higher energy level to a lower energy level creates a release of energy usually in the form of radiation, but also via the Auger process. There are also scattering events that can occur when X-rays interact with matter. Elastic scattering events occur when a photon interacts with the electrons of a sample and a photon of the same frequency, but different direction is emitted. In an inelastic scattering situation, the frequency of the emitted photon and the incident photons is not the same, and in general the emitted photon has lower frequency.

The X-ray matter interaction is described by the total absorption coefficient μ:

$\mu = \tau + \sigma$, where τ is the true absorption coefficient and σ is the scattering coefficient. The true absorption coefficient relates to the photoelectric effect when a core electron is ejected and carries excess kinetic energy. The scattering coefficient consists of the x-ray photons that can be deflected from the original direction they travel, with or without a loss of energy and with or without a collision. The scattering coefficient is usually negligible.

One of the interactions of photons and electrons with matter is X-ray photoionization in which a photoelectron is ejected from the core level after absorbing a photon. There are many different mechanisms of excited atom relaxation, these are fluorescence X-rays, Auger electrons and secondary electrons. By relaxation mechanism, we mean a method for de-excitation of the atom. In x- ray fluorescence the inner shell vacancy is filled by outer shell electrons. This process is a radiative process and the energy of fluorescence is the difference in energy between the two shells. For example, an L shell electron can fall into the K level causing a K_α fluorescence line. Next, the Auger effect is an important relaxation mechanism for an excited atom. The Auger effect is a radiation less process in which an electron drops from a higher shell to a lower shell and simultaneously ejects an electron from the same shell. This process is also referred to as autoionization. Auger transitions occur with a high probability and emit two or more Auger electrons simultaneously. An Auger electron is the electron that is ejected from the shell during this process. A vacancy cascade can occur whereby continuous ionization from additional Auger processes happens. It is important to note that the vacancy cascade can only occur with core electrons. Further, a Coster-Kronig transition, which has a large transition probability, is a special case of an Auger process in which the vacancy is filled by an electron from a higher subshell of the same shell. If the Auger electron belongs to the same shell, then this is called a super Coster-Kronig transition. The selection rules for the Auger transition is that the initial and final system must have the same symmetry and parity. It is important to note that a selection rule is a formal constraint that governs the transition from one quantum state to another.

Next, a secondary electron process can occur. This process is nonradiative and x-ray photons eject electrons when they leave the atom. The primary photoelectrons are Auger electrons.

EXAFS is essentially the region beyond the absorption edge in which oscillatory behavior occurs. In order to utilize EXAFS properly, the atoms investigated must not be isolated, since EXAFS depends on the neighboring atoms. The utilization of synchrotron radiation pioneered EXAFS as an experimental tool, which is especially useful when other methods are difficult or impossible to conduct, such as diffraction. The pre-edge region is useful because it contains information regarding bonding and electronic configuration. The absorption edge region contains information about charge. Transmission is one of the experimental modes of EXAFS measurements, but there are many others. In the transmission mode, EXAFS only includes X-ray measurements but for other modes electrons might be involved. Some of these other modes are: 1). SEXAFS, which is focused on Auger electrons, 2). EELS, which is electron energy loss spectroscopy.

EXAFS results because of the scattering process of an outgoing photoelectron by the neighboring atoms. The ejected electron behaves like a spherical wave, and we have a resulting outgoing and incoming interference from this process, since a wave is produced from the backscattering of neighboring atoms. Interference, which results from the superposition of two waves, can be coherence or destructive. The interference gives rise to the oscillatory behavior in the EXAFS region of the absorption spectrum. As a simple example in understanding EXAFS, consider a monatomic gas, like Argon. In this case, there are no neighboring atoms so the mathematics governing EXAFS is simplified:

$\lambda = \frac{2\pi}{k}$ and $KE = \frac{p^2}{2m} = \frac{\hbar^2 k^2}{2m}$ and

$k^2 = \frac{(E-E_0)(2m)}{\hbar^2}$,

so $k = (\frac{(E-E_0)(2m)}{\hbar^2})^{\frac{1}{2}}$.

The Debye-Waller factor describes the attenuation of x-ray scattering in thermal motion. Structural and chemical information can be obtained from the Debye-Waller factor.

Beer's law:

$I = I_0 e^{-\mu t}$, where I and I_0 are intensities, μ is the absorption coefficient and t is the sample thickness. We also note that μ is proportional to $\frac{I}{I_0}$.

$$\chi(E) = \frac{\mu(E) - \mu_0(E)}{\mu_0(E)}$$

where $\chi(E)$ is the fine-structure function, $\mu(E)$ is the measured absorption coefficient, $\mu_0(E)$ is a background function which is smooth and represents the absorption of an isolated atom.

Section IV: Introduction to Ferroelectric Materials

Ferroelectricity is important to realize in materials because it means the material will be useful in memory applications as CMOS technology and the like. Ferroelectricity is the characteristic of materials that have a spontaneous electric polarization that can be reversed by an application of an external electric field.[5] In order to discuss ferroelectricity, one must discuss polarization of materials. Polarization is the dipole moment per unit volume in a material. A dielectric is an insulator that exhibits electric polarization. When dielectrics are placed in an electric field, current flows in them because they have no loosely bound electrons that may drift through the material and thus electric polarization occurs. The positive charges within the dielectric are slightly displaced in the direction of the electric field, and the negative charges are displaced slightly in the direction opposite of the electric field. In materials there are several polarization materials: electronic, ionic, high-frequency dipolar, low-frequency dipolar, interfacial-space charge at electrodes and interfacial-space charge at heterogeneities such as grain boundaries. For ferroelectric materials, the high-frequency dipolar mechanism dominates.

Hafnia is well known for its high dielectric constant which is usually about 40 or 50. Hafnia is known as a refractory material, which is a material that is thermally insulating known to withstand high temperature without degrading. A linear dielectric is a material in which the dielectric polarization is linearly related to the electric field and the dielectric constant is not dependent on the electric field. Dielectric strength is the maximum electric field that can be maintained between two conductor plates without causing breakdown. It is well known that dielectric properties can only be found with certain crystal symmetries. For example, a

piezoelectric material does not possess an inversion center and is thus noncentrosymmetric. Piezoelectric materials are materials in which a stress applied to the crystal will change the electric polarization. All crystals that are ferroelectric are also piezoelectric. Ferroelectric and pyroelectric materials are noncentrosymmetric and possess a unique polar axis. A pyroelectric material is a material in which as heat is applied the electric polarization changes.

For dielectrics, the polarizability must come from either ionic or electronic contributions. Ionic polarizability can make the largest contribution in ferroelectrics. It is important to note that in a ferroelectric material the polarization does not disappear when the external field is removed, and the direction of the polarization is reversible. The internal electric dipoles of a ferroelectric material are physically tied to the material lattice, so if a change occurs in the physical lattice, a change of the strength of the dipoles and can cause current to flow into or out of the capacitor even without the presence of external voltage across the capacitor. Ferroelectrics also have a nonlinear relationship between polarization(P) and electric field(E). Hysteresis is an important feature of a ferroelectric material. Hysteresis is the dependence of a state of a system on its history and is seen as a loop in the P v. E graphs for ferroelectric materials. Spontaneous polarization is a function of temperature, as spontaneous polarization decreases with an increase in temperature and vanishes at the Curie temperature.

Section V: Landau Theory of Phase Transitions

The Curie temperature is the temperature above which materials lose permanent magnetic properties. The Curie temperature is denoted and is also referred to as the Curie point. Some ferroelectric crystals have no Curie point because they melt before leaving the ferroelectric phase. Here we must also discuss the Landau theory of phase transitions as ferroelectric materials may be classified based on first or second order phase transitions. A first order phase transition is based on the idea that the free energy can be expanded as a power series in the order parameter which is m. For second order phase transitions, the order parameter increases from zero at the phase transition and the first few terms of the power series will dominate. If the free energy is expanded to the sixth order in the order parameter, the system will undergo a first order phase transition if α_0>0, $\beta < 0$ and γ >0.

$$f(T) = f_0(T) + \alpha_0(T - T_c)m^2 + \frac{1}{2}\mathrm{B}m^4 + \frac{1}{3}\gamma m^6\alpha_0 > 0, \mathrm{B} < 0, \gamma > 0.$$

$f_0(T)$ describes the temperature dependence of the high temperature phase near the phase transition. The order parameter m minimizes the free energy:

$$\frac{df}{dm} = 0 = 2a_0(T - T_c)m + 2\mathrm{B}m^3 + 2\gamma m^5$$

One solution is m= , so cancel one factor of m:

$$0 = 2\alpha_0(T - T_c) + 2\beta m^2 + 2\gamma m^4$$

And solving further can be found in: [14]

The reason we introduce the Landau theory of phase transitions here is because we may wish to investigate the thermodynamic properties of a ferroelectric crystal. When attempting to calculate the free energy of other thermodynamic properties, the calculation can be tedious because we first must calculate the density of states. In an effort to curtail this tedious process, one must use calculations based on Landau's theory of phase transitions, i.e. expansion of a power series as an approximation for the order parameter. The order parameter is used to measure how ordered a system is, and is zero above a phase transition and nonzero below. Order parameters are also important because they can visually distinguish a first order phase transition from a second order phase transition.

The most common thermodynamic properties we are concerned with when working with ferroelectrics are the dielectric susceptibility and dielectric displacement. The dielectric susceptibility measures the degree in which a ferroelectric material polarizes in response to an applied electric field. The dielectric displacement is essentially the displacement measure of the spontaneous polarization for a ferroelectric material. Consider the following relation between Gibb's free energy and polarization:

$$G = \left(\frac{\alpha}{2}\right)P^2 + \left(\frac{\beta}{4}\right)P^4 + \left(\frac{\gamma}{6}\right)P^6 - EP$$

G is Gibb's free energy, P is polarization, α is a temperature dependent coefficient, β and γ are temperature independent coefficients, and E is the electric field. We find the minimum of the Gibb's free energy with respect to polarization, recalling how to find a minimum from calculus:

$$\frac{dG}{dP} = 0, E = \alpha P + \beta P^3 + \gamma P^5$$

Section VI: History of Ferroelectric Materials

In 2011, Boscke et al.[6] discovered experimentally that silicon doped HfO2 thin films of 10 nm thickness are ferroelectric. Mueller et al. demonstrated that PE curves of thin $Hf_{1-x}Zr_xO_2$ films in the concentration range of 0<= x <=1 with the result that HfO_2 is a linear dielectric. Ferroelectricity is thickness dependent and disappears in thicker films. This demonstrates the size effect, which is when ferroelectricity disappears in thicker films. In contrast, ferroelectric perovskites are ferroelectric in thicker films but lose electric characteristics under thin film conditions. The surface energy may explain the size effect since it depends on surface area. Boscke et al. also demonstrated the relationship between piezoelectricity and ferroelectricity via capping electrodes. Mechanical encapsulation inhibits the tetragonal phase of Si:HfO2 and led to creation of the orthorhombic phase which is ferroelectric. Additionally, in 2012 Muller et al. investigated thin $Hf_{1-x}Zr_xO_2$ films experimentally showing that pure HfO2 is a linear dielectric, meaning in HfO2 the polarization is linearly related to the electric field. Many other studies were

carried out from diverse groups and found ferroelectricity in $Hf_{1-x}Zr_xO_2$ or doped HfO_2 thin films manufactured with different deposition techniques like ALD, chemical solution deposition, sputtering or pulsed laser deposition. From Shuvalov, the point symmetry mm2 displayed by $Pca2_1$ and $Pmn2_1$ phases, the point symmetry m displayed by Pm and Cc phases, and the symmetry 1 displayed by the P1 phase are three ferroelectric subgroups of the 4/mmm tetragonal point group. The symmetry requirements for ferroelectric phases that result from parent nonpolar phases through distortions are definitive.

In 2014, Huan et al. demonstrated the ability to systematically and computationally identify ferroelectric phases of a given material system. Using a minima-hopping method to identify low-energy phases at different pressures and temperatures and then using group theoretical symmetry reduction principles which were established by Shuvalov, one is able to identify the ferroelectric phases of the system. The minima-hopping method is an algorithmic technique that finds the global minima for energy in a condensed matter system. Utilizing this method, Huan et al. was able to find that the $Pca2_1$ and $Pmn2_1$ orthorhombic space group are ferroelectric.

Crystal System	Point Group	Space group number	Abbreviation
Monoclinic	$P2_1/c(2/m)$	14	m-phase
Orthorhombic	$Pbca(mmm)$	61	o-phase
Orthorhombic(polar)	$Pca2_1(mm2)$	29	p-o-phase
Orthorhombic(polar)	$Pmn2_1(mm2)$	31	p-o'-phase
Tetragonal	$P4_2/nmc(4/mmm)$	137	t-phase
Orthorhombic	$Pnma(mmm)$	62	o'-phase
Cubic	$Fm\bar{3}m(m\bar{3}m)$	225	c-phase

Table 1.1 Space groups, point groups, space group number and abbreviation for phases of Hafnia

High k dielectrics have various applications in the semiconductor industry and essentially extend Moore's law and prevent leakage effects. Moore's law describes the doubling of transistors in microchips which leads to increased speed and capability in computers. In complementary metal-oxide semiconductors, leakage can occur because of quantum tunneling effects. Complementary metal-oxide semiconductors are continually downsized by reducing the thickness of gate insulators, and CMOS[1] is technology used for constructing integrated circuits. The leakage problem can be solved by using an insulator with a dielectric constant higher than SiO_2, this would allow for an increased physical thickness of the gate insulator. Hafnia exhibits a switchable spontaneous electric polarization which indicates this is a ferroelectric material with a high dielectric constant[2].

There are many different phases of Hafnia: monoclinic, tetragonal, cubic and orthorhombic. Starting with the monoclinic phase of Hafnia, Hafnia undergoes phase transitions which result in different space groups. The temperature at which the tetragonal phase is induced is 2000 K and cubic phase is induced at 2900 K[1]. Different dielectric constants vary from phase to phase. The average dielectric constants are highest for the cubic and tetragonal phases. In order to force a high temperature phase to be stable in Hafnia, one would need to introduce cation dopants.

Ferroelectricity in Hafnia is often investigated as the origins are not fully understood yet. The origin of ferroelectricity in Hafnia is most likely due to the noncentrosymmetric polar phase[3],

which is stable under certain conditions. The Pca2_1 orthorhombic phase is specifically shown to be stable. Ferroelectricity in Hafnia rises from creation of the polar orthorhombic phase (Pca2_1) during a rapid annealing process and a capping electrode[3]. Ferroelectricity is dependent on a variety of factors, including: Doping species, concentration, annealing temperature, film thickness.

Results

Ferroelectricity was first measured in Si-doped HfO_2 by Boscke et al, and in many following studies the influence of various dopants on ferroelectricity and pyroelectricity in $Hf_{1-x}Zr_xO_2$ was investigated experimentally and computationally. Dopants influence phase stability and provide a method to induce ferroelectricity in otherwise unstable phases. In doping Hafnia with Al, ferroelectricity is more efficiently induced in the orthorhombic phases. A geometry optimization was done with Vienna ab initio Software Package(VASP) and using generalized gradient ascent(GGA) with a projected augmented wave(PAW). The basis cutoff was 500 eV and was expanded as a 2x2x2 supercell constructed from optimized substitutions. In order to determine the correct basis cutoff, a cutoff convergence test was conducted by varying the energy cutoff with the ground state energies to find a minimum value. We can see from Figure 9 that the energy cutoff's effect on the ground state becomes constant at 400 eV.

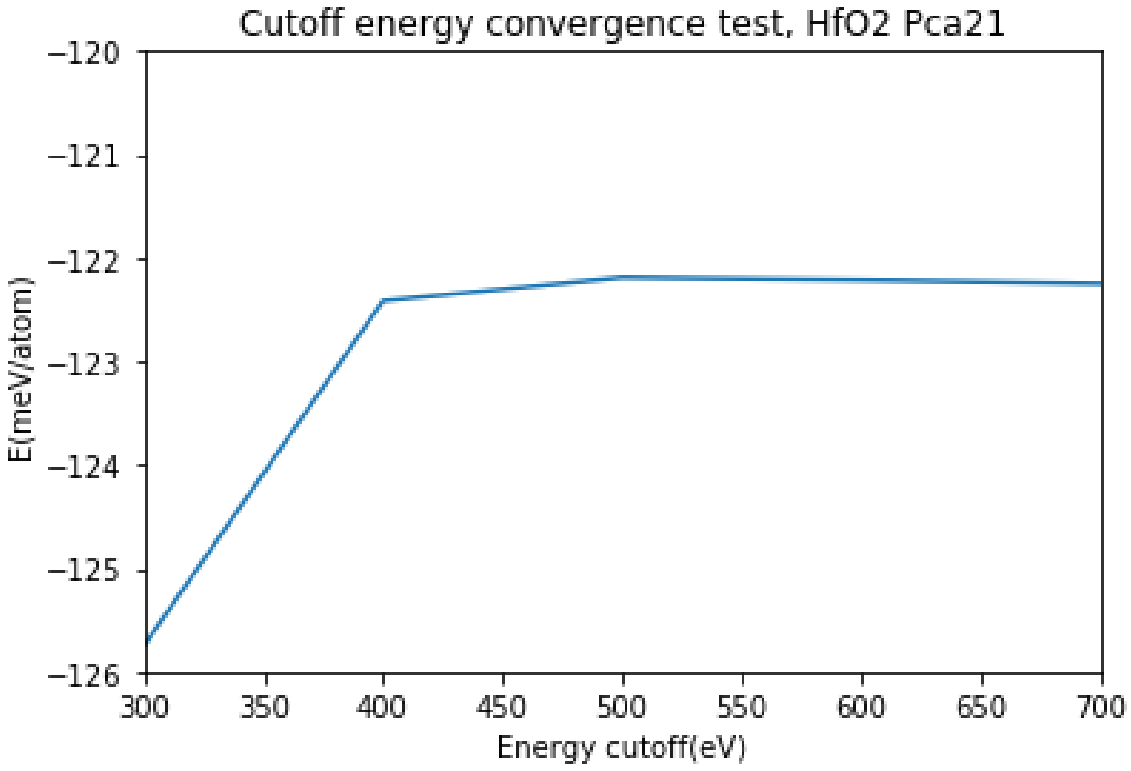

Figure 2: Energy cutoff convergence test

The initial hafnia structure was created in Materials Studio for each phase. Then, the Al was introduced as replacing one of the hafnium atoms. In the 3% geometry optimization, the structure as generated by a 2x 2 x2 supercell, resulting in 32 Hf atoms and 64 O atoms. One of the Hf atoms was replaced, resulting in $\frac{1}{32}$ which is 3.1%. After doping the system, a geometry optimization was carried out. Using a basis cutoff of 500 eV and GGA PAW potentials, an optimized structure was realized. For the 6% optimization, a supercell of 2x2x1 which contains 16 Hf atoms and 32 O atoms. In this case, replacing one hafnia atom yields 6.1%, since $\frac{1}{14}$ is about 6.1%. After doping the 6% system, the system was geometrically optimized using a basis cutoff of about 500 eV. For the 5% case, a supercell of 5 x 1 x1 results in $\frac{1}{20}$, since one of the 20 Hf atoms is replaced by Al. In order to calculate the percentage of Al in the system, given an n x n x n supercell, for hafnia one calculates n * n * n * 4. This number dictates the total number of Hf atoms in the system and the number of O atoms is determined through doubling the amount of Hf atoms. We take the number of Hf atoms and replace it by a certain number x of Al atoms, introducing the dopant to the system. Then, we calculate $x/(Hf\_total)$ * 100 to determine the percentage of Al in the system.

The Brillouin Zone points were sampled using the Monkhorst-Pack method, which consists of an evenly spaced grid of points in k space. The Brillouin Zone is the simplest cell one can create in reciprocal space. Reciprocal space is the Fourier transform of real space, and it is important to note that properties in the real space are inverse in reciprocal space, and reciprocal space is often called k-space. If the lattice is large in real space, then the lattice will be small in reciprocal space, if the lattice is small in real space, then the lattice will be large in reciprocal space. Points

in the Brillouin Zone, which are to be sampled for DFT calculations, are denoted as k-points. Sampling from a large number of k-points i.e. 20,000 or more means more accurate results from the DFT calculations. However, using a large number of k-points can decrease the speed of the calculations.

Further, we did a comparison on the accuracy of LDA v. GGA for calculating ground state densities for all Hafnia phases. The accuracy between LDA and GGA is widely discussed in [2] and we can see in Figure 12 that the LDA is overestimating the ground state density whereas GGA underestimates the ground state density. The difference in accuracy is a product of the approximations within the LDA and GGA methods.

Initial Lattice Parameters(Å)	Final Lattice Parameters(Å)
13.7	14.95135
13.7	12.78889
11.2	11.57454

Initial Angles	Final Angles
90	91.4673
90	91.8008
90	91.0374

Table 1.2 and **Table 1.3**: Pre DFT calculation and post DFT calculation, lattice parameters and angles after convergence for $Pca2_1$ 3% AlHfO2

Initial Lattice Parameters(Å)	Final Lattice Parameters(Å)
26.22	26.20115
5.07957	5.08186
5.03739	5.03876

Initial Angles	Final Angles
90	90.7421
90	89.9838
90	89.6810

Table 1.3 and Table 1.4: Orthorhombic Al:HfO2 5% Pca21, lattice parameters and angles

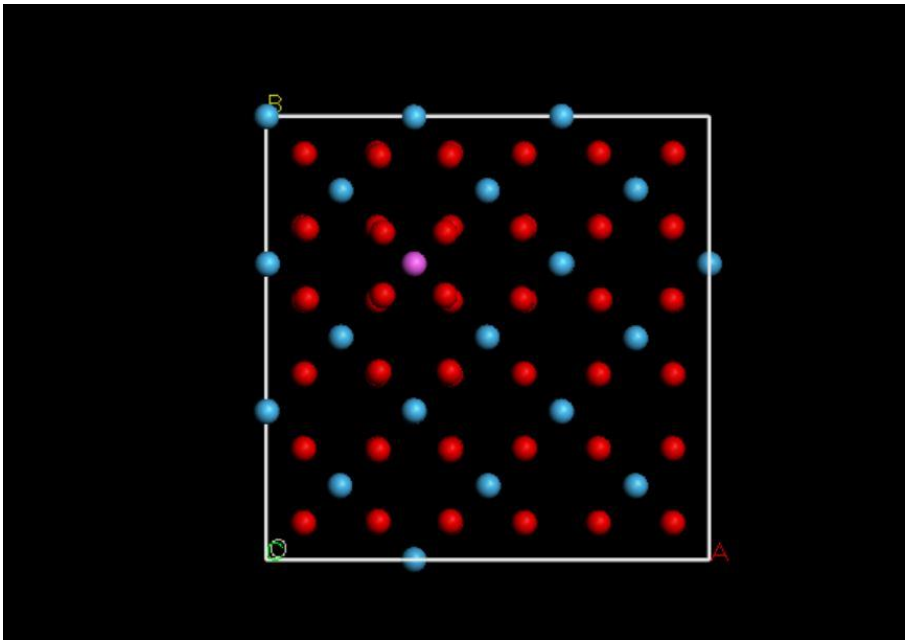

Figure 3: AlHfO2 5% Pca21, generated with Materials Studio 5.5

Initial Lattice Parameters(Å)	Final Lattice Parameters(Å)
10.13331	10.15058
10.48552	10.41357
5.08267	5.07747

Initial Angles	Final Angles
90	90.5027
90	89.8666
90	90.4377

Table 1.5 and 1.6: Orthorhombic Al:HfO2 6% Pca21, lattice parameters and angles

Ground State Energy	Percent doped
-0.129893904605E+04	3
-.76074319E+03	5
0.1153662E+02	6

Table 1.7: Ground State Energies: Tetragonal Al:HfO2

Ground State Energy	Phase(Al:HfO2)
-.12251836E+03	Monoclinic($P2_1/c$)
-.36498480E+03	Rhombohedral(R3)
-.36517657E+03	Rhombohedral(R3m)

Table 1.8: Ground State Energies for Monoclinic and Rhombohedral Al:HfO2

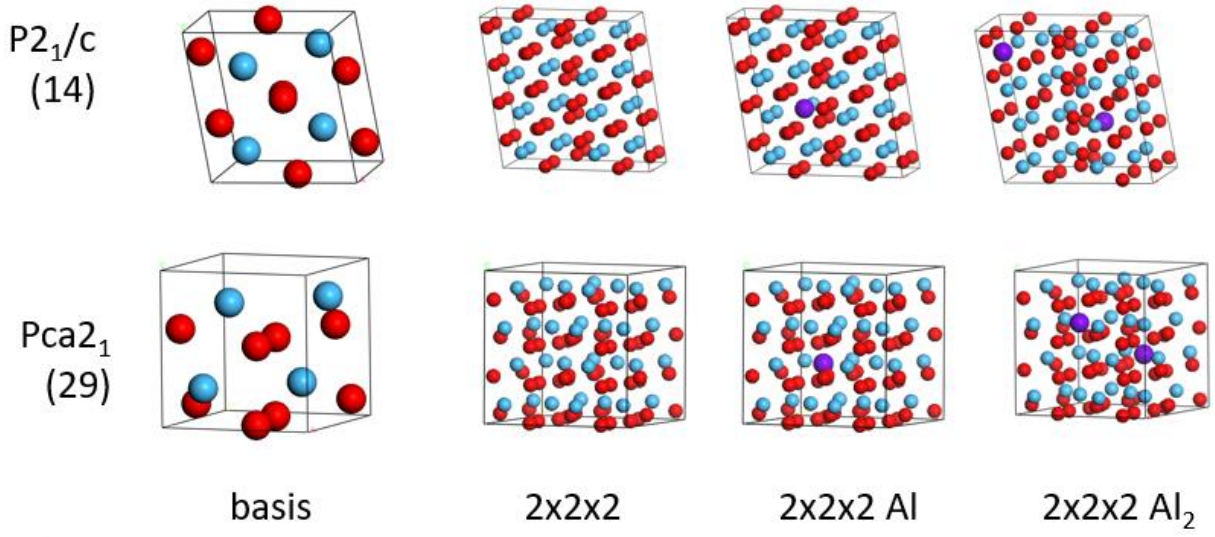

Figure 4: P21/c and Pca21 AlHfO2, generated with Materials Studio 5.5

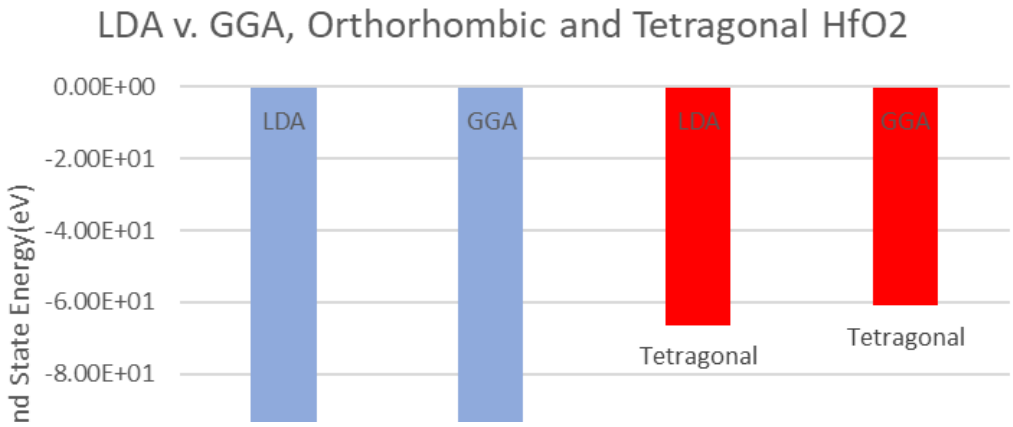

Figure 5: LDA v. GGA, Orthorhombic and Tetragonal HfO2

Conclusion

In this study, we focused on geometric relaxations of Al doped HfO_2 systems in order to use with EXAFS data. $HfO_2$was doped with Al in order to help control the ferroelectric phases in HfO_2. It is generally understood that the orthorhombic phases of Hafnia are ferroelectric, but others are not. In order to dope the system, Materials Studio software was used to replace one Hf atom with Al for various doping percentages. The percentages focused on in this study were 3%, 5% and 6%. The different phases investigated in this study were the monoclinic, tetragonal and orthorhombic. After doping the system, VASP was used to perform DFT calculations for different meshes, and configurations. Our goal was to geometrically optimize the system by pushing it to the minimum free energy.

After running the geometric optimizations, we obtained good convergence which works well with the EXAFS fits. There were two main sources of data for this study: EXAFS fits and cif files generated from DFT calculations. The EXAFS fits represent the experimental portion of the study and the cif files represent the theoretical portion.

References

[1] M. Dogan, N. Gong, T-P. Ma, S. Ismail-Beigi, Causes of ferroelectricity in HfO_2- based thin films: an ab initio perspective, arXiv, 2019

[2] J.G. Lee, Computational Materials Science: an Introduction (CRC Press, Taylor & Francis Group, Boca Raton, 2017)

[3] W. G. Laidlaw, Introduction to Quantum Concepts in Spectroscopy, (McGraw-Hill 1970)

[4] I.N. Levine, Quantum Chemistry (Pearson Education, Upper Saddle River, NJ, 2009).

[5] C. Kittel, Introduction to Solid State Physics (Wiley, New York, 1956).

[6] T.S. Böscke, J. Müller, D. Bräuhaus, U. Schröder, and U. Böttger, Applied Physics Letters 99, 102903 (2011).

[7] J. Müller, T.S. Böscke, U. Schröder, S. Mueller, D. Bräuhaus, U. Böttger, L. Frey, and T. Mikolajick, Nano Letters 12, 4318 (2012).

[8] T. Tsuneda, Density Functional Theory in Quantum Chemistry(Springer Japan, 2014)

[9] D.A. MacQuarrie, Quantum Chemistry (Univ. Science Books, Sausalito, CA, 1985).

[10] Huan, T. D., et al. (2014). "Pathways towards ferroelectricity in hafnia." Physical Review B 90(6).

[11] R. Batra, T.D. Huan, G.A. Rossetti, and R. Ramprasad, Chemistry of Materials 29, 9102 (2017).

[12] U. Schroeder, E. Yurchuk, J. Müller, D. Martin, T. Schenk, P. Polakowski, C. Adelmann, M.I. Popovici, S.V. Kalinin, and T. Mikolajick, Japanese Journal of Applied Physics 53, (2014).

[13] B.K. Teo, EXAFS: Basic Principles and Data Analysis (Springer, Berlin, 1986).

[14] G. Bunker, Introduction to XAFS: a Practical Guide to X-Ray Absorption Fine Structure Spectroscopy (Cambridge University Press, Cambridge, UK, 2010).

[15] S. Calvin and K.E. Furst, XAFS for Everyone (CRC Press, an imprint of Taylor & Francis Group, Boca Raton, FL, 2018).

[16] P.A.M. Dirac, Special Relativity and Quantum Theory 157 (1988).

[17] D. C. Koningsberger and R. Prins, Xray Absorption: Principles, Applications, Techniques of EXAFS, SEXAFS, and XANES (Chemical Analysis 92, John Wiley & Sons, 1988).

[18] G. Kresse and J. Hafner. Ab initio molecular dynamics for liquid metals. (Phys. Rev. B, 47:558, 1993

[19] G. Kresse and J. Hafner. Ab initio molecular-dynamics simulation of the liquid-metal-amorphous-semiconductor transition in germanium. (Phys. Rev. B, 49:14251, 1994)

[20] G. Kresse and J. Furthmüller. Efficiency of ab-initio total energy calculations for metals and semiconductors using a plane-wave basis set. (Comput. Mat. Sci., 6:15, 1996)

[21] G. Kresse and J. Furthmüller. Efficient iterative schemes for ab initio total-energy calculations using a plane-wave basis set. (Phys. Rev. B, 54:11169, 1996)

[22] P. E. Blochl. Projector augmented-wave method. (Phys. Rev. B, 50:17953, 1994)

[23] G. Kresse and D. Joubert. From ultrasoft pseudopotentials to the projector augmented-wave method. (Phys. Rev. B, 59:1758, 1999)

[24] J.P. Perdew, J.A. Chevary, S.H. Vosko, K.A. Jackson, M.R. Pederson, D.J. Singh, and C. Fiolhais. Atoms, molecules, solids, and surfaces: Applications of the generalized gradient approximation for exchange and correlation. (Phys. Rev. B, 46:6671, 1992)

[25] J.P. Perdew, J.A. Chevary, S.H. Vosko, K.A. Jackson, M.R. Pederson, D.J. Singh, and C. Fiolhais. Erratum: Atoms, molecules, solids, and surfaces: Applications of the generalized gradient approximation for exchange and correlation. (Phys. Rev. B, 48:4978, 1993)

[26] J. Evans, X-Ray Absorption Spectroscopy for the Chemical and Materials Sciences (John Wiley & Sons, Inc., Hoboken, 2018).

[27] S. Choi, T. Shiraishi, T. Kiguchi, T. Shimizu, H. Funakubo, and T.J. Konno, Applied Physics Letters 113, 262903 (2018)

[28] T. Shiraishi, K. Katayama, T. Yokouchi, T. Shimizu, T. Oikawa, O. Sakata, H. Uchida, Y. Imai, T. Kiguchi, T.J. Konno, and H. Funakubo, Applied Physics Letters 108, 262904 (2016)

[29] Y. Xiao and K. Bhattacharya, Smart Structures and Materials 2004: Active Materials: Behavior and Mechanics (2004)

[30] V. Blum, R. Gehrke, F. Hanke, P. Havu, V. Havu, X. Ren, K. Reuter, and M. Scheffler, Computer Physics Communications 180, 2175 (2009)

[31] S.V. Ushakov, C.E. Brown, and A. Navrotsky, Journal of Materials Research 19, 693 (2004)

[32] M.W. Pitcher, S.V. Ushakov, A. Navrotsky, B.F. Woodfield, G. Li, J. Boerio-Goates, and B.M. Tissue, Journal of the American Ceramic Society 88, 160 (2004)

[33] W. Zhou, S.V. Ushakov, T. Wang, J.G. Ekerdt, A.A. Demkov, and A. Navrotsky, Journal of Applied Physics 107, 123514 (2010)

[34] X., S., et al. (2015). "On the structural origins of ferroelectricity in HfO2 thin films." Appl. Phys. Lett. 106: 162905.

[35] Y. Wei, P. Nukala, M. Salverda, S. Matzen, H.J. Zhao, J. Momand, A.S. Everhardt, G. Agnus, G.R. Blake, P. Lecoeur, B.J. Kooi, J. Íñiguez, B. Dkhil, and B. Noheda, Nature Materials 17, 1095 (2018).